



Fault reactivation in brittle–viscous wrench systems—dynamically scaled analogue models and application to the Rhine–Bresse transfer zone

Kamil Ustaszewski^{a,*}, Markus E. Schumacher^a, Stefan M. Schmid^a, Dick Nieuwland^b

^aDepartment of Earth Sciences, University Basel, Bernoullistrasse 32, CH-4056 Basel, Switzerland

^bDepartment of Tectonics and Structural Geology, Faculty of Earth and Life Sciences, Vrije Universiteit, De Boelelaan 1085, 1081 HV Amsterdam, The Netherlands

Received 14 August 2003; accepted 24 March 2004

Abstract

Analogue experiments on oblique rifting and subsequent transpressional reactivation were performed with two-layer slabs of sand and silicone. In this brittle–viscous system, transtensional and transpressional wrench faulting was induced by movements of a basal rigid plate. The dynamically scaled analogue models are confronted with the structural evolution of the Rhine–Bresse transfer zone (RBTZ) that linked Palaeogene rifting in the Upper Rhine and Bresse Grabens and that appears to have been transpressively reactivated in Neogene to recent times. Fault patterns produced in the sand layer above the basal silicone layer are compared with structural elements in the sedimentary cover, separated from the basement by an evaporitic décollement layer.

In order to investigate strain-rate dependence of fault reactivation and graben inversion, transpressional shortening was performed under different displacement rates. Experimental results suggest that the reactivation of pre-existing structures in a brittle cover above a viscous décollement is strongly dependent on the strain rate within the viscous layer. Under low to intermediate displacement rates (2.6 cm h^{-1}), deformation concentrates within the basal viscous layer and former normal faults within the cover are not reactivated. The reactivation at higher displacement rates (5 cm h^{-1}) results in a complete inversion of graben structures within the cover. Ongoing shortening produces lobed thrust fronts, which crosscut pre-existing normal faults.

Late Pliocene to recent en-échelon aligned folds and isolated thrust faults in the cover of the RBTZ are attributed to thick-skinned reactivation of basement faults. A comparison of natural and experimentally obtained structures suggests that fault reactivation occurred under low displacement rates ($< 1 \text{ mm/a}$). This results in a low mechanical coupling between basement and cover in areas with significantly thick décollement layers, providing an explanation for decoupled stresses between basement and cover, such as observed in the northern Jura Mountains.

© 2004 Elsevier Ltd. All rights reserved.

1. Introduction

1.1. Objectives and previous modelling work

Selective reactivation of pre-existing crustal fault segments is a phenomenon frequently observed at various scales, because it can occur at local stresses

lower than those needed for the creation of new faults (cf. Fig. 17 in Richard and Krantz, 1991). In general, faults represent surfaces of reduced or negligible cohesive strength. Their reactivation is basically controlled by the coefficient of friction and the pore fluid pressure. Hence, reactivation of pre-existing faults occurs if the resolved shear stress along a fault plane is large enough to exceed frictional resistance (Byerlee, 1978). This requires the principal stresses to be in a favourable orientation with respect to the trend of the pre-existing fault.

*Corresponding author. Tel.: +41-61-267-0909; fax: +41-61-267-3613.

E-mail address: kamil.ustaszewski@unibas.ch (K. Ustaszewski).

A number of experiments on fault reactivation have been performed in previous studies. Most of this work focused on basement-driven reactivation of faults, usually simulated in analogue experiments by introducing a basal discontinuity in the model, which triggers and localises deformation in the overlying cover (Richard and Krantz, 1991; Nalpas et al., 1995; Brun and Nalpas, 1996; Dubois et al., 2002). Because of the higher resolved shear stress, transpressional reactivation of normal faults within the cover occurs more easily than pure compressional reactivation. Hence, reactivation is favoured if the direction of the greatest principal stress σ_1 is oblique to the fault trend. Reactivated basement faults, which lead to reactivation of structures in the cover, exhibit a substantial wrench component (Richard and Krantz, 1991). Brun and Nalpas (1996) found that reactivation of graben-bounding normal faults requires an angle of less than 45° between the compression direction and the fault trend, and that inversion becomes even more significant at angles lower than 30° . Dubois et al. (2002) have performed experiments on normal fault reactivation in brittle–viscous systems, adding sand layers during deformation. Their results suggest that the kinematics of reactivated normal faults also depend on the thickness of the sedimentary overburden above the basement fault.

The strain-rate dependence of the strength of viscous horizons (e.g., evaporites), often found between basement and cover, is an additional important parameter. It influences the coupling between basement and cover. Hence, strain rate, which controls the transmission of stresses between brittle and ductile/viscous layers, also becomes very important. In this case, reactivation also depends on the rheology of the viscous materials involved. Hitherto little attention has been paid to this effect and experiments were usually performed at constant strain rates (e.g., Schreurs and Colletta, 1998).

In this study, we will also address the strain rate dependence during transpressional reactivation of normal faults in brittle–viscous systems, keeping the geometry constant throughout all experiments. The results of the model will be applied to a natural example, the Rhine–Bresse transfer zone (RBTZ) of the European Cenozoic Rift System. There, Middle Triassic evaporites act as a regional décollement horizon between the pre-rift sedimentary cover and the basement. This transfer zone accommodated predominantly transtensive motions during Palaeogene times (Lacombe et al., 1993; Schumacher, 2002). The area also bears evidence for late Neogene to recent shortening and uplift, which is most presumably linked to basement-induced transpressional fault reactivation in its sedimentary cover, as will be discussed below. Deformation rates for this phase of reactivation are rather ill-defined in the field, but can be estimated on the base of our dynamically scaled sand–silicone models.

1.2. Regional geology and evidence for thick-skinned reactivation

The RBTZ represents a major W–E trending intra-continental transfer zone within the Cenozoic rift system of Europe (Fig. 1a). It connects late Eocene to Oligocene extension in the Upper Rhine graben (URG) with contemporaneous extension in the Bresse graben. This rifting implies coeval sinistral transtensional movements along the RBTZ (Laubscher, 1970; Bergerat and Chorowicz, 1981; Illies, 1981; Lacombe et al., 1993). Pre-existing Late Variscan and Permo-Carboniferous WSW–ENE trending fault systems are responsible for the localisation of transfer zones and for the structural segmentation of the European Cenozoic rift system. Most important in this context is a set of fault-controlled troughs of Permo-Carboniferous age, generally trending parallel to this Variscan structural grain. Important additional pre-existing structures are Palaeozoic NNE–SSW- (“Rhenish”) and NW–SE-oriented (“Hercynian”) faults. Palaeogene transtensional movements, controlled by pre-existing structures in the basement, were accommodated by the formation of numerous ENE- to NNE-striking normal faults in the Mesozoic sedimentary cover, and, additionally—owing to the presence of evaporites at the base of the Mesozoic succession—by flexures. Basement faults within the RBTZ crop out only in the Massif de la Serre (labelled “MS” in Fig. 1a). This small basement horst is bounded by ENE- and NE-trending normal faults in the north and south, respectively, which were active in the Late Palaeozoic and reactivated during Palaeogene transtension (Chauve et al., 1983; Coromina and Fabbri, 2003). Subcrop maps showing the Permo-Carboniferous trough system (Diebold and Naef, 1990; Laubscher and Noack, 1997) and Variscan lineaments (Debrand-Passard and Courbouleix, 1984), as well as our work based on industry seismic reflection data, point towards the existence of numerous, NE- to ENE-striking ($N45^\circ E$ – $N80^\circ E$) faults in the subsurface of the RBTZ and the southernmost URG. Geomorphologic, geological and geophysical data give evidence for Late Pliocene to recent uplift and shortening in the RBTZ and the southernmost Upper Rhine Graben, summarised below.

1.2.1. Geomorphologic data

Differential vertical movements between the area of the transfer zone and the Upper Rhine Graben since the Late Pliocene (Post 2.9 Ma; Liniger, 1963; Petit et al., 1996; Giamboni et al., 2004) can be inferred from the abandonment of the riverbed of the Palaeo-Aare, which drained westward across the Sundgau into the Bresse depression in Middle Pliocene times (4.2 to 2.9 Ma; Petit et al. 1996), and the associated capture of the Rhine into the Rhine Graben. These drainage network changes were accompanied by shifts in the location of Quaternary

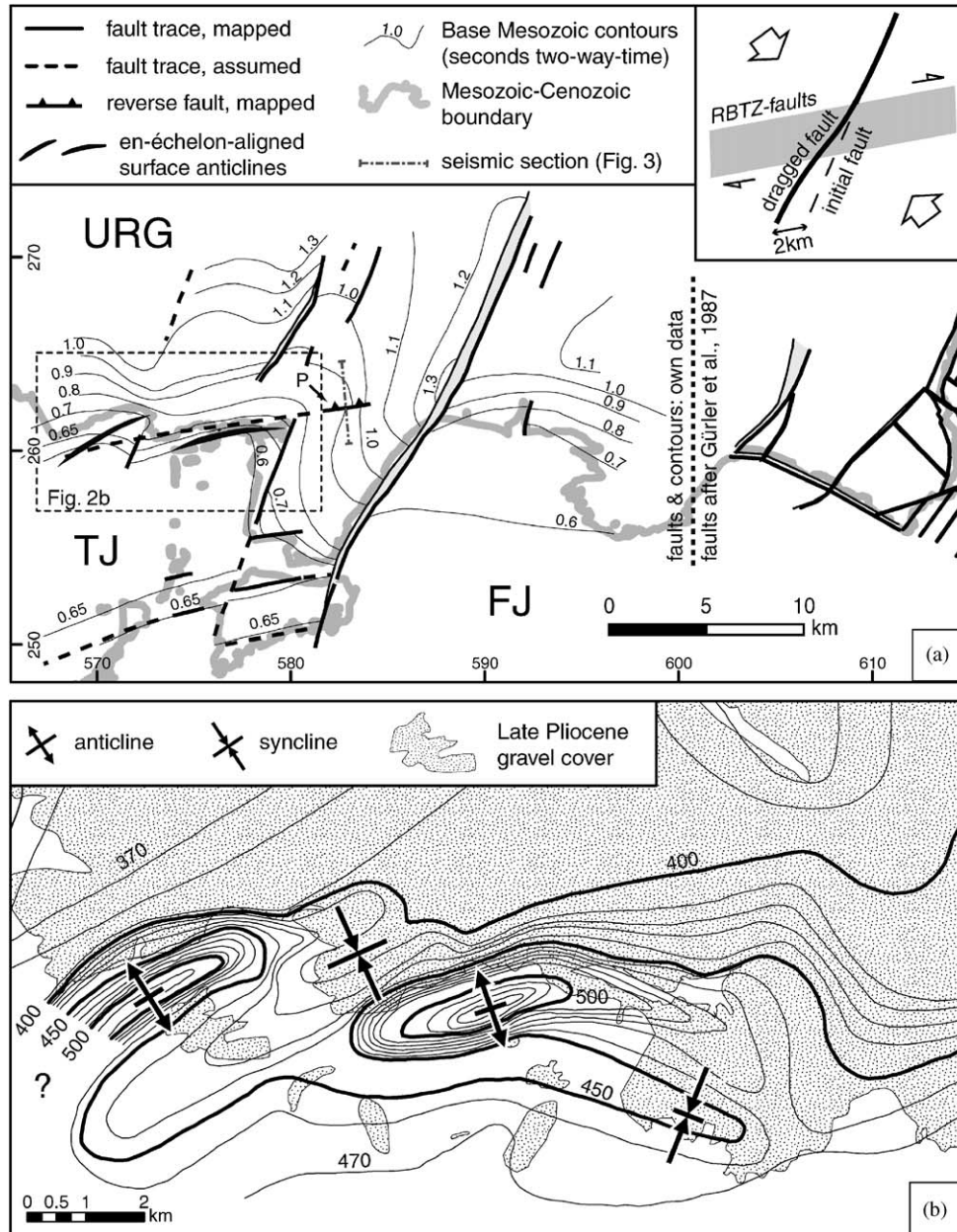


Fig. 2. (a) Close-up on a part of the southernmost Upper Rhine Graben (URG) and adjacent Jura Mountains, showing faults dissecting the Base Mesozoic (western part) and Top-Buntsandstein surfaces (eastern part of figure). Note the systematic dextral drag of N20°-trending faults along ENE-trending faults, which is interpreted as the result of dextral reactivation of ENE-trending faults in the Neogene (insert at top right). Numbers at edges refer to Swiss National grid. FJ=Folded Jura, TJ=Tabular Jura, P=Pfetterhouse reverse fault. (b) Contours of the base of Late Pliocene Sundgau gravels (in m above sea level; isohypse distance 10 m) in the area of en-échelon aligned surface anticlines, testifying to Post-Late Pliocene to recent shortening (after Giamboni et al., 2004).

testifying to Late Pliocene to recent shortening of the sedimentary cover (Giamboni et al., 2004; Fig. 2b). Systematically northward tilted Pleistocene river terraces of Rhine tributaries in the Sundgau (Nivière and Winter, 2000) and immediately north of the Avant Mont thrust (labelled “AM” in Fig. 1a) along the Ognon River (Goguel and Dreyfuss, 1967; Dreyfuss and Kuntz, 1970; Campy, 1984) give additional support to the

hypothesis that uplift and shortening within the RBTZ has remained active during the Quaternary.

1.2.2. Recent stress field

While WNW–ESE-oriented extension prevailed in the RBTZ in the Eo- to Oligocene, it was subjected to NW–SE- to WNW–ESE-oriented compressive stresses since the early Miocene (Lacombe et al., 1993 and

Fig. 1b). These reoriented stresses, exerted from the nascent Alps in the south, led to the cessation of rifting in the southern URG. During the Late Miocene to Lower Pliocene, the southernmost parts of the RBTZ were incorporated into thin-skinned Jura folding and thrusting. The present day stress field in parts of the Folded Jura Mountains and their foreland, however, appears incompatible with presently ongoing Jura décollement tectonics, because currently observed maximum horizontal stresses (inferred from in-situ stress measurements) deviate up to 90° from the σ_1 -directions during the main stage of Jura folding (Becker, 2000; and references therein). Additionally, the reoriented recent stress directions extend far into the non-detached foreland. This led Becker (2000) to exclude ongoing décollement tectonics in the sense of Laubscher (1961). The maximum horizontal stresses in the cover of the RBTZ are NW–SE- to WNW–ESE-oriented (black double arrows in Fig. 1a), making pre-existing ENE-oriented faults prone to dextral reactivation. The maximum horizontal stresses in the seismogenic basement of the southern URG and adjacent areas reveal a consistent NW–SE-orientation (Plenefisch and Bonjer, 1997; Deichmann et al., 2000). However, in the detached cover of the northern Jura Mountains, maximum horizontal stresses are more N–S oriented (Müller et al., 1987; Becker, 2000), indicating that stresses between cover and basement are still decoupled there (compare black and white double arrows in Fig. 1a).

The ENE-striking, north-verging Avant-Mont thrust (“AM” in Fig. 1a), is an isolated thrust fault in the autochthonous Mesozoic, traceable for almost 50 km along strike. It nucleated most presumably above a pre-existing fault formed during Eo-/Oligocene transtension and has been hitherto regarded as the outermost thrust of the “thin-skinned” Jura fold and thrust belt (Philippe, 1995). On the other hand, it is yet unclear how the Avant-Mont thrust is geometrically and kinematically linked to the detached Mesozoic of the thin-skinned Jura fold belt. In the west it appears to terminate against an Oligocene normal fault, delimiting the Massif de la Serre horst (“MS” in Fig. 1a) to the south. Towards the east, shortening along it progressively diminishes until becoming insignificant. In-situ-stress measurements indicate WNW-directed maximum horizontal stresses (Fig. 1a), making the Avant-Mont thrust prone for accommodating a combined reverse- and dextral motion in a “thick-skinned” manner. Other isolated thrust faults in the autochthonous Mesozoic such as the Avant-Mont thrust are found east of Basel (e.g., Mandach and Mettau thrusts, “M” in Fig. 1a; Wildi, 1975; Laubscher, 1986, 1987). Although their development was generally attributed to the nucleation of décollement-related thrusts and folds above pre-existing faults and flexures in the basement (Wildi, 1975; Laubscher, 1977, 1986, 1987; Müller et al., 2002) their

geometrical link with the detached Mesozoic of the Folded Jura Mountains is as questionable as in the case of the Avant-Mont thrust.

1.2.3. Subsurface data

Fig. 2a depicts faults offsetting the Base Mesozoic surface in the southernmost part of the Upper Rhine Graben, which were active during Eo-/Oligocene extension. They were independently mapped by different authors (Gürler et al., 1987; Ustaszewski et al., in press) on the base of reflection seismic profiles. Fig. 2a shows that the approximately $N20^\circ$ trending faults reveal a conspicuous and systematic dextral drag where they approach the ENE-trending faults delineating the RBTZ. These faults affect a stratigraphic level situated below the Triassic décollement horizon. Thus, this drag cannot be explained by compression and/or wrenching related to thin-skinned Jura thrusting/folding, which only affected the detached sedimentary cover but not the Base Mesozoic surface. At the surface, two en-échelon anticlines are situated exactly above ENE-trending basement faults, which have gently folded the base of the Pliocene Sundgau gravels (Giamboni et al., 2004; Fig. 2b). Eastward, a reverse fault trending ENE in the along-strike continuation of the en-échelon-aligned anticlines was mapped in the subsurface of the Oligocene fill within an adjacent graben (labelled “P” in Figs. 2a and 3). Fig. 3 shows a reflection seismic line traversing this reactivated ENE-trending fault. An extensional flexure has developed in the Mesozoic sediments above a steeply north-dipping normal fault during Eo- to Oligocene rifting. This normal fault delimits a Permo-Carboniferous trough, as depicted by differently reflective basement beneath the Mesozoic sediments across the fault. Synrift sediments, tapering southward, are of Upper Priabonian to Late Chattian age. Compressive or rather transpressive reactivation of the normal fault led to the inversion of the flexure. This is evidenced in the gently folded Upper Rupelian reflector (marked “R”). According to the seismic information available (Fig. 3), fault reactivation could have occurred as early as in the Late Chattian. Seen in a larger context, however, reactivation rather occurred after the establishment of NW–SE-oriented greatest principal stress in Aquitanian times (Laubscher, 1992; and Fig. 1b, right). The evidence provided in Figs. 2 and 3 shows that dextral reactivation of ENE-oriented basement faults in the RBTZ has inverted formerly extensional flexures in the cover, leading to dextrally dragged $N20^\circ$ trending faults (top right insert in Fig. 2a).

The geomorphologic, geological and geophysical observations described in this section testify to Neogene (particularly Upper Pliocene to recent) thick-skinned tectonic activity in the RBTZ. We intended to compare natural structures with experimentally obtained ones by

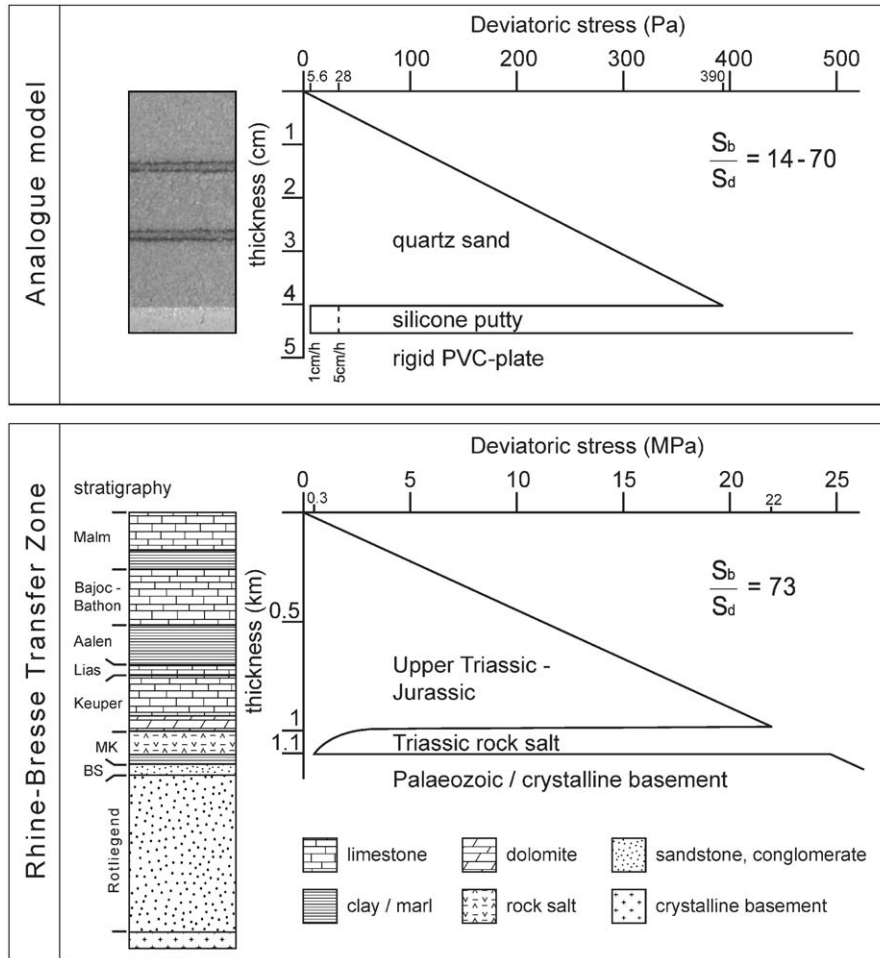


Fig. 4. Strength profiles for the dynamically scaled experiments (top) and the RBTZ (bottom) using a simplified stratigraphy for the Mesozoic pre-rift series based on various borehole data. Abbreviations: BS = Buntsandstein, MK = Muschelkalk.

boreholes (Schmidt et al., 1924; Häring, 2001; Fig. 4, bottom). This pile of sediments predominantly consists of limestones, which responded to rift-related extension mainly by brittle failure. Intercalated Aalenian shales are considered as brittle layers in our modelling since they reveal no transition from cataclastic to plastic behaviour with increasing differential stresses (Nüesch, 1991). Therefore, they are unlikely to have had any significant effect for strain partitioning during rifting. However, viscous behaviour is expected for the Triassic Muschelkalk and Gipskeuper series, where rock salt, anhydrite and/or gypsum predominate. While the Gipskeuper contains frequent shale intercalations, very pure and up to 80 m thick rock salt is present in the basal Triassic Muschelkalk series. For convenience, we assumed an overall thickness of viscous rock salt of 100 m, which yields a thickness ratio of brittle to viscous sediments on the order of 10:1 in the overall stratigraphic column.

The basement consists either of crystalline rocks or of Permian clastic deposits (sandstone, quartzite and conglomerate). Both revealed brittle behaviour in their

top part during Palaeogene rifting as can be inferred from the cataclastic behaviour of these rocks, where they are exposed along the URG-border faults.

3. Experimental setup

Sand–silicone models were built in order to investigate the effects of basement fault reactivation on the deformation of a brittle sedimentary cover above a basal viscous décollement layer. Two successive deformation stages were applied: an initial phase of oblique rifting with sinistral transtensional motion and a subsequent phase of dextral transpressional reactivation (Fig. 5). The analogue models were dynamically scaled for the sedimentary pile overlying a Palaeozoic basement in the area of the southern Upper Rhine Graben and the RBTZ. They match the natural “prototype” in terms of yield stresses acting on brittle and viscous materials during Eocene–Oligocene rifting (see Fig. 4 for the strength profiles obtained and Appendix for details regarding dynamical scaling).

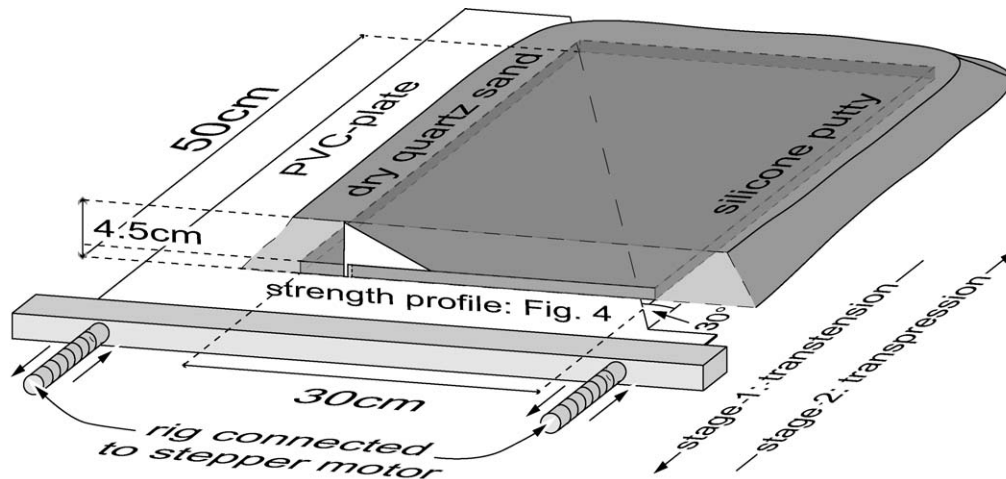


Fig. 5. Schematic block diagram of the experimental setup. A rectangular block of silicone putty ($50 \times 30 \times 0.5$ cm) is entirely covered by 4 cm of dry quartz sand. Deformation in the two-layer model is induced by a 1 mm thick, rigid basal PVC plate, which is driven by an electronically controlled stepper motor.

The analogue models were underlain by a 1 mm thin, rigid PVC plate, which was cut at an angle of 30° to the extension direction (Fig. 5). The oblique edge of the plate represents a pre-existing discontinuity, which induces deformation in the covering sand. A basal layer of silicone putty, 50×30 cm large and 5 mm thick, was placed above this discontinuity. The silicone putty including its edges was entirely covered by 4 cm of dry quartz sand, in order to prevent gravitational sideward flow of silicone (Fig. 5). Coloured marker layers of sand were sprinkled in defined steps in order to visualise vertical displacements across faults. A rectangular grid of coloured sand lines with a spacing of 5 and 7.5 cm, respectively, was sprinkled on the smoothed surface of the model in order to visualise lateral displacements induced during the experiment.

Computer-controlled stepper motors imposed the deformation on the rig. Displacement rates during the experiment run ranged from 1 to 5 cm/h. Top view photographs were taken at several steps during the different experimental runs, allowing for tracing fault evolution during each deformation increment. After completion of the experiment, the model was covered by an additional layer of sand in order to seal its relief, and subsequently sprinkled with water, until the pore space was saturated. This provided the necessary cohesion for cutting the model into slices, perpendicular to the trend of the pre-existing discontinuity in the PVC plate. Photographs were taken from all sections.

4. Experimental results

Two-phase experiments were performed under varying displacement rates (see Table 1 for technical parameters). Displacement rates during the first defor-

mation phase (transtension) were performed at 1 and 2.6 cm/h (Fig. 6). The subsequent phase of transpressional reactivation was performed at displacement rates of 1, 2.6 and 5 cm/h, in order to vary coupling across the viscous layer by a factor of 5 (see Appendix A). One experiment (OR4, Figs. 7 and 8) was terminated after completion of the first transtensional stage in order to compare purely transtensional structures to those caused by subsequent transpressive reactivation. In the following two Sections (4.1 and 4.2), we describe the sequential development of structures seen in top view during experimental runs and in cross sections for three experiments (OR4, OR5, and OR7).

4.1. Stage 1 (transtension)

The first surface faults appear in the brittle cover after 3–5 mm displacement (Fig. 6a). Forming right above the basement fault with a spacing of typically 2–3 cm (measured perpendicular to the fault trend), they display a right-stepping en-échelon alignment and sinistral, oblique slip sense of motion as deduced from the displacement of the grid lines at the model surface. The polarity of the normal fault component switches precisely above the basal pre-cut discontinuity (Fig. 6a). These en-échelon faults are oriented at angles between 15° and 20° to the basement fault and may be interpreted as synthetic Riedel (R) shears (Fig. 6a). Such angles are quite typical of wrench faults with transtensional kinematics (cf. Mandl, 1988, p. 77).

Progressive deformation widens the fault zone by along-strike propagation of the en-échelon faults, usually away from the basement discontinuity (Fig. 6). During this widening, individual faults begin to overlap each other (Fig. 6b and c). Their ends often become fringed and slightly curved, facilitating fault coalescence

Table 1
Parameters of analogue experiments performed

Experiment	v1	v2	S_b	S_d	S_b/S_d	Displ1	Displ2	New fts 1	React. fts 2	New fts 2	Figures
OR1	5.0	5.0	490	28	18	18	50	R, P	Both R & P	New thrusts	
OR2	5.0	5.0	392	28	14	29	60	R, P	Both R & P	New thrusts	
OR3	1.0	1.0	392	5.6	70	20	61	R, P	None	None	
OR4	2.6	—	392	15	26	20	—	R, P	—	—	7, 8
OR5	2.6	2.6	392	15	26	20	65	R, P	Mainly P	Few thrusts	9, 10
OR6	2.6	2.6	294	—	—	10	35	Only R	Only R	Thrusts	
OR7	1.0	5.0	392	5.6	70	20	60	R, P	Both R & P	New R & thrusts	6, 11, 12
OR8	1.0	2.6	392	5.6	70	20	60	R, P	Mainly P	None	

Experiments and resulting fault patterns. Experiments referred to in text and figures are shown in bold italics. v1 = displacement rate during stage 1 (cmh^{-1}), v2 = displacement rate during stage 2 (cmh^{-1}), S_b = strength of brittle layers (Pa), S_d = strength of viscous layer (Pa), S_b/S_d = strength ratio, displ1 = displacement during transtensive stage (mm), displ2 = displacement during transpressive stage (mm), new fts 1 = neo-formed faults at stage 1, react. fts 2 = faults reactivated at stage 2, new fts 2 = neo-formed faults at stage 2, R = R-shear, P = P-shear.

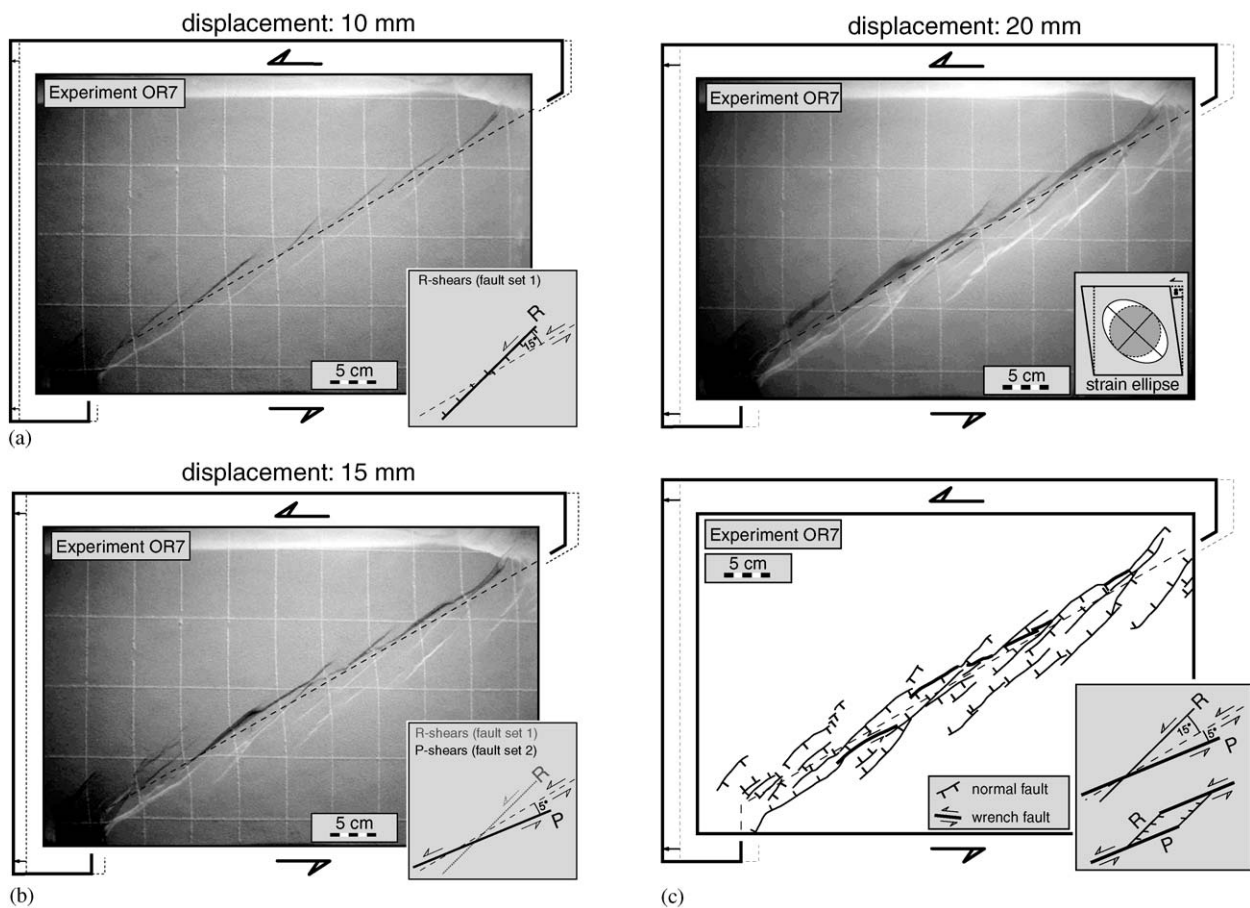


Fig. 6. Stepwise development of surface faults during oblique rifting at a displacement rate of 1 cm/h (transtensional phase of experiment OR7). Illumination from top part of figure. (a) Surface faults forming first (after 10 mm displacement) are en-echelon aligned, synthetic R-shears. Note the switch in fault polarity right above the trace of the basement fault. (b) After 15 mm displacement, a set of P-shears appears. (c) Coalescence of the two fault sets (after 20 mm transtension) allows for the formation of lozenge-shaped pull-apart basins (schematically shown by insert at lower right).

as deformation advances. Due to this fringing, the angle between basal discontinuity and the outermost tips of en-echelon fault segments may increase to 30–35°. Fault formation always progresses from outside to inside the rift. This is depicted in three cross-sections cut through

an experiment that was terminated after the transtensive stage (OR4, Fig. 8).

Between 5 and 10 mm displacement, a second fault set appears at the surface, trending either sub-parallel to the basement discontinuity or at an angle as small as 5° (but

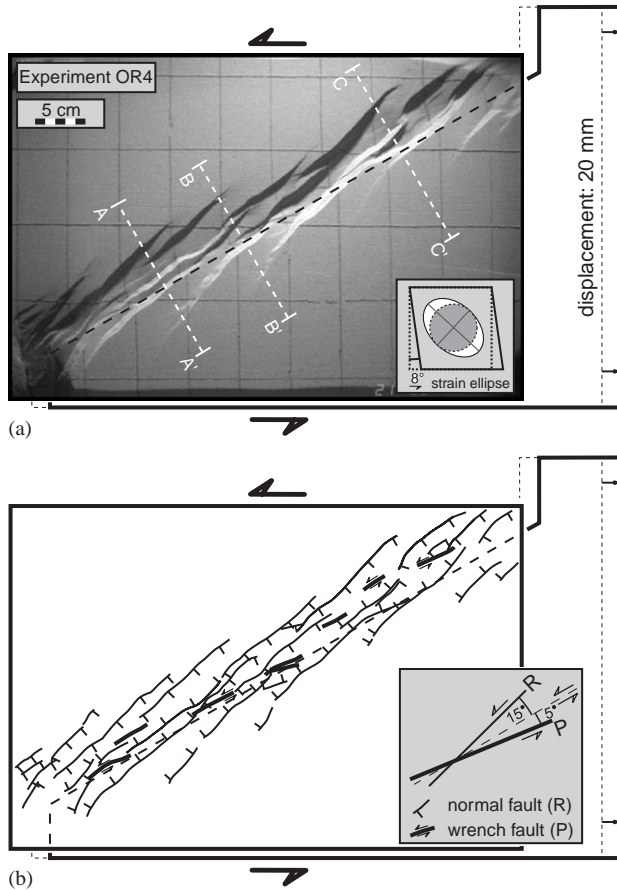


Fig. 7. Oblique rift model (transensional wrench faulting, experiment OR4). Illumination from top part of figure. (a) Fault pattern and representative strain ellipse after 20 mm transensional displacement. Locations of cross-sections (Fig. 8) are indicated. (b) Line drawing of the fault pattern. Note the switch in normal fault polarity with respect to the location of P-shears.

in the opposite direction compared to earlier formed R-shears). Displacements are primarily sinistral, the vertical throw being significantly smaller than in case of the first fault set. These faults are interpreted as P-shears (Fig. 6b). The linkage of individual faults of these two sets leads to the formation of small, lozenge-shaped pull-apart basins (Fig. 6c). Fault dips range between 65° – 80° for both sets of faults, the viscous basal layer being visibly thinned below the graben structure (Fig. 8).

The total displacement was restricted to 20 mm in most experiments. At this stage, the oblique rifts did not develop into a continuous graben structure, which would have complicated the tracing of movements during subsequent reactivation. The final fault pattern after completion of the transensional stage displays an array of en-échelon aligned oblique-slip normal faults with several graben and horst structures (Fig. 6c, 7 and 9a) and—occasionally—well defined basins that formed by the linkage of R- and P-shears (Fig. 6c and 9a).

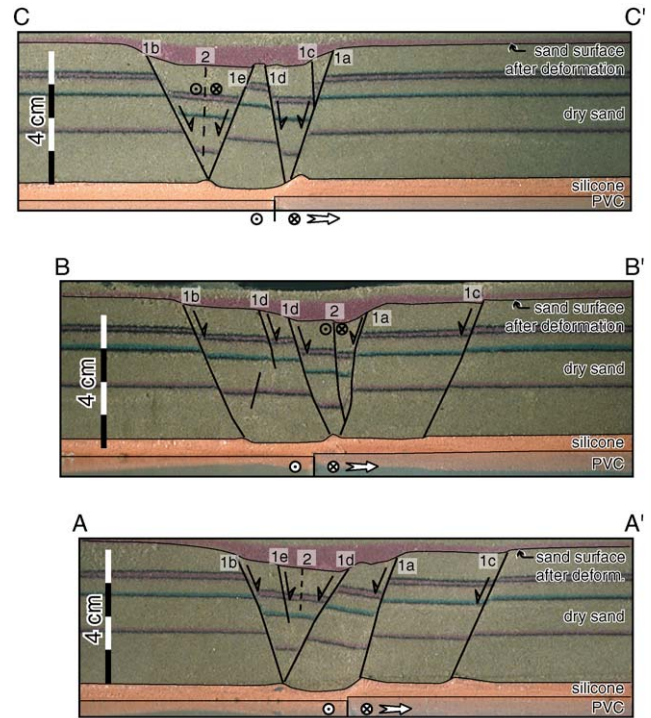


Fig. 8. Cross-sections across the oblique rift structure (experiment OR4) after 20 mm transension. For location of the sections see Fig. 7. Note the characteristic thinning or “necking” of the viscous base below the graben. Genetic chronology of faults is indicated by numbers 1 and 2. Lower case letters indicate relative chronology in which the individual faults appear in the section plane by along-strike propagation. First faults (1a, 1b) are synthetic R-type shears and form the external boundary faults of the graben. Along-strike propagation of these en-échelon aligned faults (labelled “1c”) causes widening of the rift. Younger R-type faults (1d, 1e) form in the interior part of the rift. Faults of generation 2 are P-type shears and form in the centre of the rift.

4.2. Stage 2 (transpression)

The reactivation of numerous pre-existing faults produced during the first deformation stage was only observed at high displacement rates ($v = 5$ cm/h). Transpression at lower displacement rates ($v = 1$ to 2.6 cm/h) led to strain localisation in the vicinity of the pre-cut PVC-plate, without fault inversion propagating towards the surface of the brittle cover.

4.2.1. Reactivation at low displacement rates ($v = 1$ – 2.6 cm/h)

Deformation in the sand layer concentrates along reactivated P-shears (“rP” in Fig. 9b). R-shears are not reactivated, presumably due to higher angles between fault strike and shortening direction, resulting in lower resolved shear stresses. Therefore, graben structures are not inverted, even after 65 mm of shortening (Fig. 9b). Movement along reactivated P-shears is readily seen in

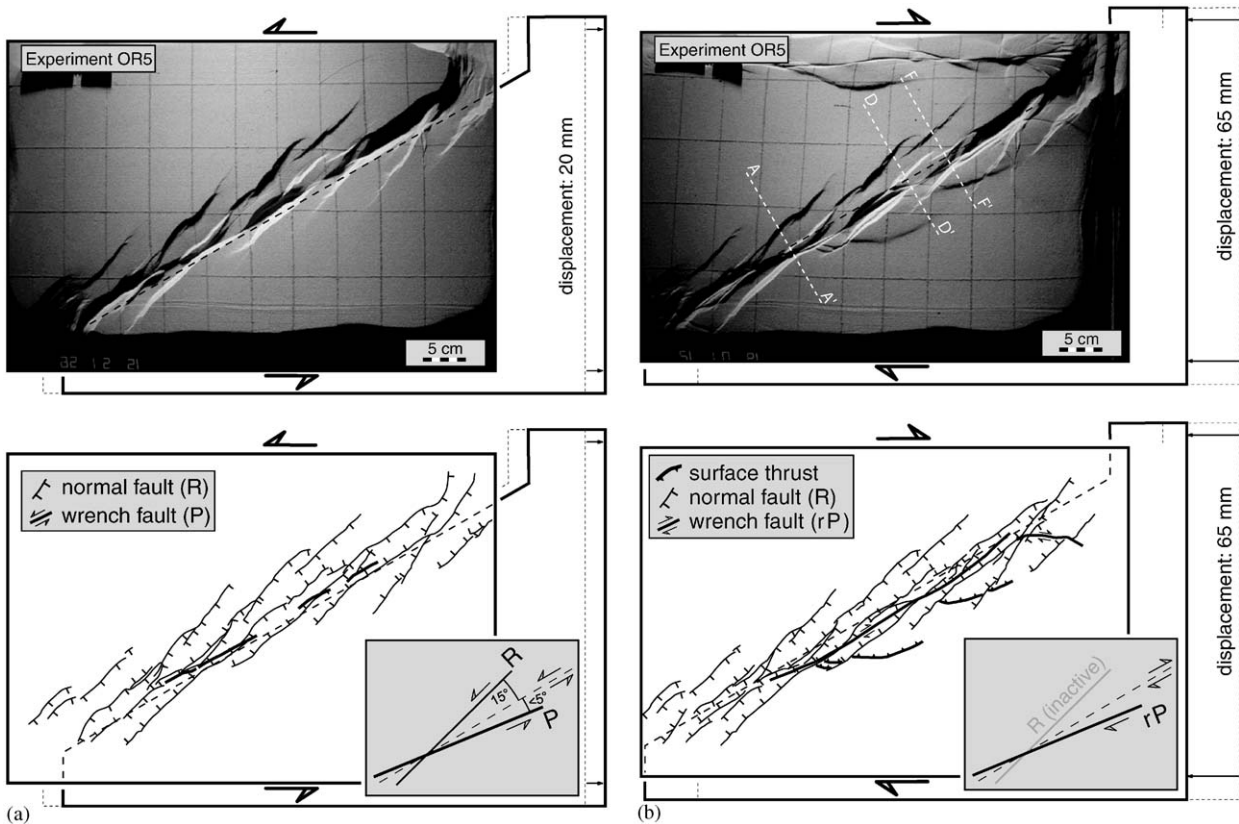


Fig. 9. (a) Fault patterns of an oblique rift model (transtensional wrench faulting, experiment OR5) after 20 mm of transtension. Illumination from top part of figure. Local depocenters are formed by linkage of R- and P-shears as well as by the corrugation of fault ends. (b) Fault pattern of the same experiment after subsequent transpressional reactivation at a low displacement rate of 2.6 cm/h and 65 mm displacement. No inversion of the graben occurred. Illumination is from above. Strike-slip fault in top-part of the picture represents boundary effect due to lateral confinement of the silicone putty, but did not affect structures evolving in central rift. Locations of cross-sections (Fig. 10) indicated. rP = reactivated P-type fault.

the displacement of the vertical marker lines (compare Fig. 9a and b). During an advanced stage of transpressional shortening (between 40 and 50 mm), small surface thrust faults appear. These thrusts are transferred along pre-existing R-type faults (Fig. 9b). Subordinate narrowing of the rift is achieved by combined reverse and dextral strike-slip faulting along reactivated P-type faults (compare Figs. 9a and b).

Cross sections reveal that the viscous material has accumulated in the vicinity of the velocity discontinuity. The characteristic necks, which formed in the silicone putty as a result of transtension (compare Figs. 8 and 10), are “filled up” during this stage. The thickening of the viscous material is slightly more pronounced on the side opposite to the indenting plate. The P-type faults in the graben centre are reactivated in dextral strike-slip mode. They show a significantly curved trace in cross section. The convergence point of both reactivated and neo-formed faults at the viscous décollement horizon is always significantly offset with respect to the location of the edge of the basal plate (Fig. 10).

Shortening during reactivation under lower displacement rates is therefore compensated predominantly by

thickening of the viscous base in the vicinity of the pre-existing basal discontinuity. Only a subordinate amount of this shortening is transferred into fault inversion within the brittle cover. There, deformation is strongly concentrated along reactivated P-shears in the rift centre, leading to the development of vertical shear-zones (cross-sections in Fig. 10).

4.2.2. Reactivation at high displacement rates ($v = 5 \text{ cm/h}$)

Reactivation of inherited faults within the brittle cover is observed from the very beginning of the transpressive deformation stage. Normal faults immediately become reactivated as dextral strike-slip faults with a reverse component (Fig. 11a). In the initial stage of reactivation, they accommodate most of the shortening, leading to the almost entire inversion of graben structures. After 35 mm displacement, almost all faults (of both R- and P-type) have been reactivated (Fig. 11a). The first surface thrust faults appear at the margin of the wrench corridor. They branch off from inherited R-type faults at the periphery of the rift and propagate away from the rift in a strongly curved, lobate-shaped manner (see “surface thrust/reverse fault” in Fig. 11a).

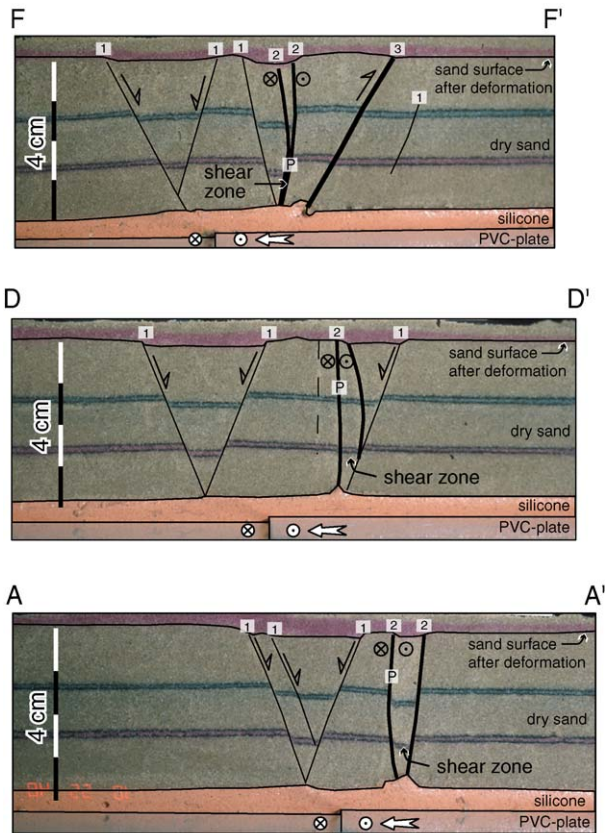


Fig. 10. Cross-sections through a transpressively reactivated oblique rift model (low displacement rate, experiment OR5). For locations see Fig. 9b. Numbers 1 to 3 indicate the nature of faults during transpressional reactivation. (1) not reactivated (R-type) faults, (2) reactivated (P-type) faults, (3) reverse faults formed during transpressional reactivation. Reactivated and neo-formed faults are drawn with thicker stroke. Note the slightly thickened silicone in the vicinity of the edge of the basal plate.

After 60 mm displacement (end of experiment, Fig. 11b), the former oblique rift has been uplifted along thrust faults that have propagated away from the basement fault to either side. Thrust fronts have widely coalesced and paralleled the basal discontinuity. The strain ellipse indicates shortening of the original rift width by some 25%, significantly more than during reactivation at low displacement rates. Newly formed dextral, synthetic Riedel-type strike-slip faults (at angles of 20–25° with respect to the basal discontinuity) branch off from inherited R-type faults and tend to link with reactivated P-shears in the interior part of the oblique graben. This gives the resulting coalesced structure a slightly sigmoidal shape (Fig. 11b).

In cross-section (Fig. 12), the neo-formed reverse faults reveal a dip angle of only 40–45°, i.e., considerably less than the dip of inherited normal faults. Most of the shortening is taken up by the neo-formed reverse faults as soon as they appear at the surface of the model. Reactivated faults reveal much less activity from this

point onward. In cross sections, neo-formed reverse faults emanate from the pre-existing basement discontinuity. As they propagate towards the surface, they intersect and offset inherited normal faults. The offset segments are thus transported in the hanging wall of reverse faults, i.e., graben structures are not actively inverted but passively uplifted (sections A–A' to C–C' in Fig. 12). Note that in the high displacement rate experiment both reactivated and neo-formed faults converge precisely above the basal discontinuity. There, the basal silicone putty is visibly thickened and even becomes involved in thrusting. This is in great contrast to the low-displacement rate experiment (compare Figs. 10 and 12).

5. Discussion

5.1. Limitations of the models

Since the length scale ratio of our models is on the order of $L^* \approx 4 \times 10^{-5}$ (see Appendix A) the models do not encompass the entire area of the RBTZ but only represent the kinematic setting found within an area of 7.5 by 12.5 km, encompassing one or a few individual faults within this transfer zone. This limits direct comparison between experiments and natural structures. However, using a larger model area and properly scaling the thickness of the sediments at the same time, proved to be impractical.

Furthermore, the amounts of displacement applied during both stages of the experiment are highly exaggerated when compared to the RBTZ. Especially the displacements applied during stage 2 greatly exceed those observed within the RBTZ. However, large displacements were necessary in order to ease the distinction between inherited and neo-formed structures in the experiments. This again limits a direct comparison of the experiments with the RBTZ.

In order to allow for a better observation of fault patterns during all stages of the experiments, no sand was filled into the subsiding areas. Such an additional load by syn-rift sedimentation would certainly have modified the principal stresses during the transpressive stage of the experiments. As shown by Dubois et al. (2002), the sedimentary fill of the graben controls the position of the intermediate and least principal stress and—consequently—the kinematics of reactivated normal faults. Additional load increases the vertical principal stress, hence reactivated faults tend to have a more pronounced strike-slip component. Conversely, they will display a greater reverse component in the absence of additional overburden. However, since the amount of rift-related sedimentation is small within in the RBTZ, this particular restriction does not significantly limit the application of the models.

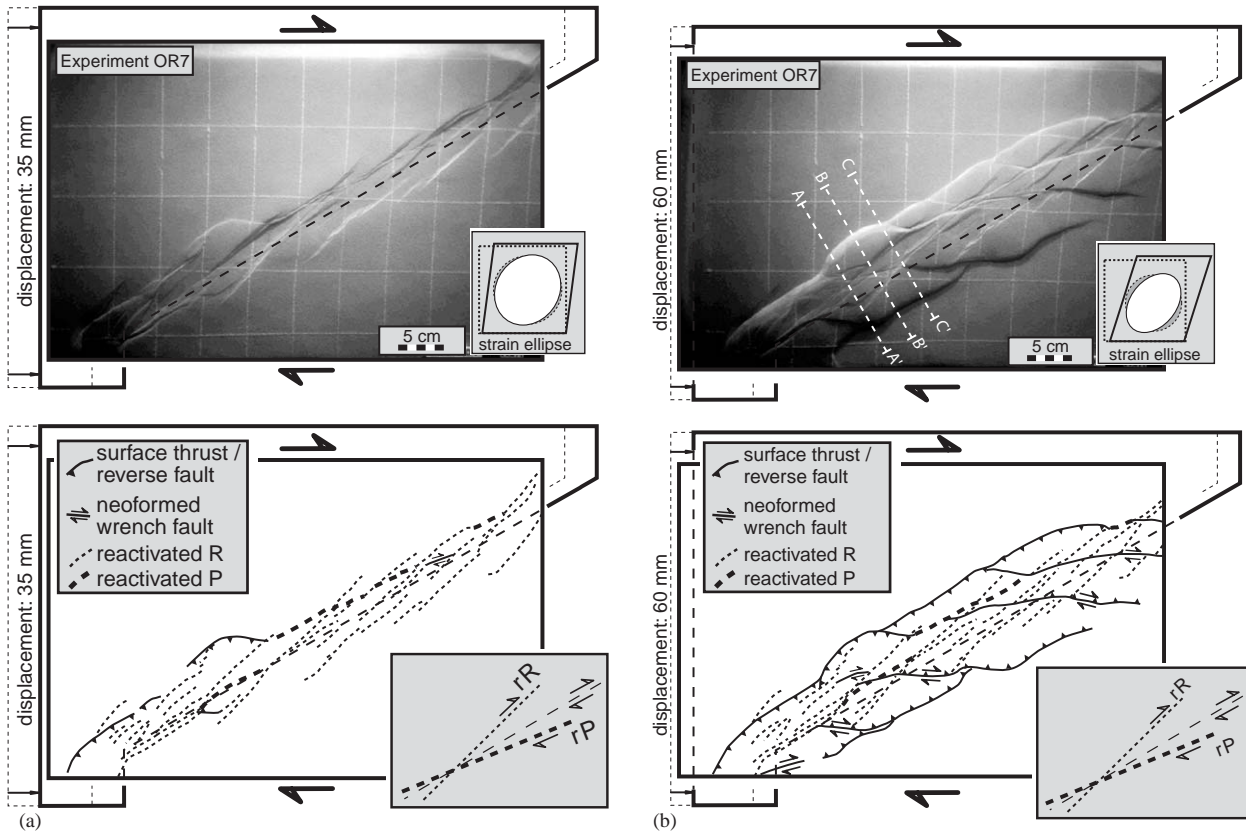


Fig. 11. Oblique rift model (transensional wrench faulting, experiment OR7), transpressively reactivated at a high displacement rate of 5 cm/h. Compare Fig. 6 for oblique rift stage before transpressional reactivation. rR = reactivated R-type fault, rP = reactivated P-type fault. (a) Deformation pattern after 35 mm of transpressive displacement. Illumination is from above. (b) Deformation pattern at the end of the experiment (after 60 mm of displacement). Illumination from top part of figure. Locations of cross-sections are indicated by dashed white lines.

5.2. Rheological and kinematic implications

Before discussing possible applications of our models to the case of the RBTZ, we discuss some important implications of general geological interest. Analogue modelling clearly showed that transpressional reactivation of pre-existing faults resulting from oblique rifting in a brittle cover overlying a viscous décollement layer is strongly dependent on the applied displacement rate.

In the low displacement rate experiments (1–2.6 cm/h) the viscous layer accommodates a large amount of shortening by ductile, i.e. not localised, deformation. Reactivation of faults in the brittle cover is insignificant except for dextrally reactivated P-shears in the rift centre. The graben itself remains non-inverted. Only few surface thrusts, which are transferred along inherited R-type faults, form during a later stage of the deformation (experiment OR5, Fig. 9b). Cross-sections (Fig. 10) reveal that the basal silicone accumulates in the vicinity of the basal discontinuity.

Conversely, reactivation of pre-existing faults is favoured under higher displacement rates (5 cm/h).

The viscous basal layer immediately transmits the shortening to the brittle cover. Almost all pre-existing faults are reactivated as dextral faults with a substantial reverse component. Graben structures, as well as pull-apart basins, are completely inverted. During an advanced stage of deformation, shortening is taken up by neo-formed thrust faults, which emanate from the basal discontinuity and propagate outward from the oblique rift. These initially strongly curved thrust faults coalesce into thrust fronts parallel to the trend of the basement fault. The thrust faults typically crosscut pre-existing normal faults with lower dip-angles (sections A–A', B–B' in Fig. 12, experiment OR7), widening the deformed belt.

5.3. Applications of the modelling results to a possible transpressive reactivation of the RBTZ

In this section, our experimental results are confronted with structures in the RBTZ. We restrict this comparison to the autochthonous Mesozoic, where shortening related to Late Miocene to Pliocene thin-skinned Jura folding can be largely excluded.

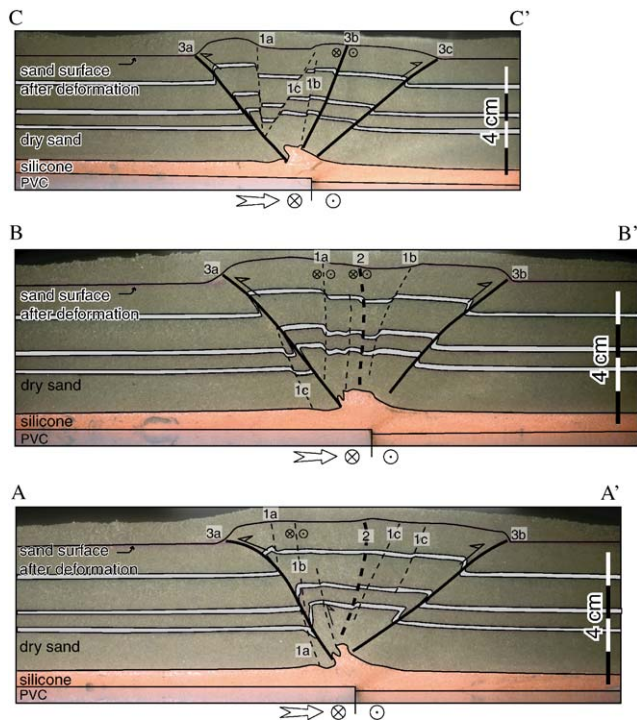


Fig. 12. Cross sections through a transpressively deformed oblique rift model (high displacement rate, experiment OR7). For locations see Fig. 11b. Numbers 1–3 indicate the nature of faults during transpressional reactivation. (1) reactivated R-type faults, (2) reactivated P-type faults, (3) neo-formed reverse faults. Lower case letters indicate relative sequence in which the individual faults appear in the section plane by along-strike propagation. Strokes and dashes correspond to Fig. 11.

As described in Section 1.2, a purely thin-skinned origin of the “Avant-Mont thrust” (“AM” in Fig. 1) in the autochthonous Mesozoic is unlikely. The Avant-Mont thrust resembles the thrust fronts, which formed during the reactivation stage in our high displacement rate experiments, trending parallel to the basal discontinuity. However, in the high displacement rate experiments such thrust fronts develop only after shortening amounts that highly exceed those expected during the postulated dextral inversion of the RBTZ (Fig. 11a, b). On the other hand, the low displacement rate experiments (OR5, Fig. 9b and 10) demonstrated that cover faults trending (sub)-parallel to the basal discontinuity are reactivated as dextral strike-slip faults over a considerable length, whereas adjacent normal faults at higher angles to the main discontinuity are not reactivated. This comes closer to the case of the Avant-Mont thrust, which forms an isolated thrust surrounded by un-inverted normal faults. In summary, a thick-skinned component during the formation of the Avant-Mont thrust at low displacement rates is very likely.

The best-documented thick-skinned reactivation of ENE-oriented faults within the RBTZ is found W of Basel (Figs. 2 and 3), the evidence being extensively discussed in Section 1.2 and in Giamboni et al. (2004).

Dextral transpressive reactivation of ENE-oriented Late Palaeozoic graben faults led to the compressive/transpressive reactivation of Palaeogene en-échelon flexures in the cover, while nearby situated N20°-trending normal faults remained largely un-inverted (Figs. 2 and 3). This local transpressive reactivation of RBTZ-faults without inversion of the graben structures resembles the situation simulated in an experiment carried out at slow displacement rates (Fig. 9b). However, the natural complexities cannot be achieved in the models (no NNE-striking basement faults were implemented into the model), hence more detailed comparisons of geometrical details are impossible.

Lobate shaped thrust segments are frequently found in the domain of the Folded Jura Mountains, especially along its northern front W of Basel (Figs. 1 and 2). It would be appealing to infer analogies to those formed during our experiments (Fig. 11a), at least from a geometrical viewpoint. However, it has been demonstrated that such thrust fronts form in the detached sedimentary cover during Mio-/Pliocene Jura folding along Eo-/Oligocene normal faults, which nucleate (thin-skinned) lateral ramps due to oblique convergence (Tschanz and Sommaruga, 1993; Philippe, 1995). Also, the experimentally produced lobate thrusts appear at shortening amounts greater than transtensional displacements, which is certainly not the case in the RBTZ.

Furthermore, the low displacement rate experiments demonstrate that, due to low coupling across the décollement layer, certain cover faults remain unaffected by motion of the basal plate. Low coupling between basement and cover may, in turn, lead to differently oriented stresses. This phenomenon is observed in the northernmost Folded Jura Mountains, where basement and cover reveal differently oriented maximum horizontal stresses (Fig. 1a, Müller et al., 1987). We believe that low displacement rates in the basement of the RBTZ (Section 1.2) and late increments of thin-skinned Jura folding (Müller et al., 2002), could explain the observed stress decoupling.

6. Conclusions

Our modelling work leads to the following conclusions:

- (1) Higher displacement rates improve coupling between basement and cover, separated by a viscous layer. This leads to “basement-triggered”, combined strike-slip/reverse reactivation of inherited R- and P-type faults in a brittle cover overlying a viscous décollement layer. Reactivation at low displacement rates, on the other hand, tends to reactivate P-shears only.

- (2) Following full inversion of pre-existing extensional structures, new lobate-shaped thrust faults develop at both high and low displacement rates. However, thrust formation is again much more pronounced at higher displacement rates.
- (3) Thrusting and uplift at low displacement rates is mostly restricted to neo-formed surface thrusts, whereas it is observed along all inverted faults at high displacement rates.

Applications of the modelling results to the RBTZ are possible, despite the limitations in the experimental setup (primarily in terms of geometrical complexity). Based on geological evidence, some Late Pliocene to recent structures can be attributed to the reactivation of ENE-trending basement faults. One such example are the reactivated Palaeogene flexures above ENE-trending faults, leading to dextrally dragged N20°-trending faults at the southern end of the Upper Rhine Graben (Figs. 2 and 3). Geological estimates of the current displacement rates (though vague) reveal values on the order of <1 mm/a. Partial stress decoupling between the basement and its sedimentary cover is presently observed in the northern Alpine foreland of Northern Switzerland (Müller et al., 1987) and in parts of the RBTZ (Fig. 1a). Hence, the experiments performed at low displacement rates (1–2.6 cm/h), characterised by weak coupling between cover and “basement”, come nearest to the situation in the RBTZ. According to the modelling this weak coupling allows for the preservation of former non-inverted normal faults. Additionally, it allows for a superposition of basement-induced dextral/reverse motions and thin-skinned, Jura type tectonics (caused by stresses exerted in the Alps and transmitted into their foreland along a basal Triassic décollement) in Late Pliocene to recent times. Combining field evidence and experimental results, it is concluded that post-Late Pliocene thrusting and uplift in the cover of the RBTZ could have resulted from strike-slip faulting along ENE-trending basement faults at low displacement rates, presumably camouflaged by late increments of thin-skinned folding in the northern Folded Jura Mountains.

Acknowledgements

Authorisation to publish reflection seismic data is the courtesy of Shell International EP. This study is a contribution to the EUCOR-URGENT (Upper Rhine Graben Evolution and Neotectonics) project and benefited from logistic and financial support of the European Union funded ENTEC (Environmental Tectonics) research and training network. We particularly acknowledge funding for K.U. by Swiss grant BBW 99-0567-1 and for M.S. by a University of Basel ELTEM grant. Dimitrios Sokoutis (Vrije Universiteit Amster-

dam) is greatly thanked for guidance in scaling techniques. Thanks are extended to Peter Ziegler (Basel) for helpful suggestions. Thorough and constructive reviews by Olivier Fabbri (Besançon) and Martin Burkhard (Neuchâtel) helped to further improve the manuscript.

Appendix A. Dynamical scaling of analogue models

Any analogue model is representative of a natural system only if it is properly dynamically scaled (Hubbert, 1937). This requires similar stress ratios acting in both model and nature, as well as appropriately downscaled rheological properties of the modelling materials. The geometries resulting from faulting in a brittle cover above ductile or viscous parts of the crust are strongly dependent on the mechanical coupling between the brittle and ductile/viscous material. This coupling can be estimated by calculating the ratio of strength between brittle and viscous/ductile parts of the crust (regardless whether lithospheric or uppermost crustal scale processes are considered) and represented graphically following the concept of Brace and Kohlstedt (1980).

For a dynamically scaled experiment, the strength ratio of the analogue model should equal that of its natural prototype within one order of magnitude:

$$\left(\frac{S_b}{S_d}\right)_{\text{model}} \approx \left(\frac{S_b}{S_d}\right)_{\text{nature}}.$$

Suffixes b and d signify properties of brittle and ductile/viscous material, respectively.

A.1. Brittle strength

The yield strength of a brittle material equals the deviatoric stress

$$S_b = \sigma_1 - \sigma_3$$

and depends upon the thickness of overburden h_b (m), its density ρ (gcm^{-3}), the internal friction angle ϕ ($^\circ$), the cohesion τ (Mpa) and the mass acceleration due to gravity, g (ms^{-2}). The letters in angular parentheses indicate the physical dimension.

In extensional regimes, the maximum principal stress (σ_1 is vertical and equals the lithostatic load:

$$\sigma_1 = p \cdot g \cdot h_b.$$

From the Mohr-Coulomb fracture criterion follows:

$$\sigma_1 = a + b\sigma_3$$

where

$$a = 2\tau_0\sqrt{b}$$

and

$$b = \frac{(1 + \sin \phi)}{(1 - \sin \phi)}.$$

An appropriate value for cohesion (τ_0) of crust under extension is 5 MPa (Byerlee, 1978).

The internal friction angle (ϕ) for most rock types is around 30° and thus $b = 3$.

Consequently,

$$a = 1.73 \times 10^7 \text{ Pa.}$$

Using values of 2.5 gcm^{-3} for the average density of the Mesozoic limestone-shale sequence of the southern Rhine Graben (see above) with a thickness h_b of 1000 m on the average, one obtains values for the maximum and minimum principal stresses of

$$\sigma_1 = 2.45 \times 10^7 \text{ Pa}$$

$$\sigma_3 = 2.41 \times 10^6 \text{ Pa}$$

and for the yield strength at the base of the sedimentary succession considered

$$S_b(\text{nature}) = \sigma_1 - \sigma_3 = 2.2 \times 10^7 \text{ Pa.}$$

Dry quartz sand reveals a Mohr–Coulomb type behaviour of failure $\tau = \tau_0 + \sigma_n \tan \phi$, an internal friction angle ϕ around 30° (Krantz, 1991) and was therefore a representative material for modelling the brittle Mesozoic sediments.

Due to negligible cohesion of sand ($\tau_0 = 0$), the brittle strength in the scaled analogue model simplifies to

$$S_b = \frac{2}{3} \cdot p \cdot g \cdot h_b$$

Using a length scale ratio $L^* \approx 4 \times 10^{-5}$, the thickness of brittle layers in the model is downscaled to $h_b = 4 \text{ cm}$.

The density of dry, sprinkled sand is 1.5 gcm^{-3} . The brittle strength thus becomes

$$S_b(\text{model}) = \sigma_1 - \sigma_3 = 392 \text{ Pa.}$$

A.2. Viscous strength

The strength of viscous material—or its resistance to (shear) deformation—depends on its viscosity μ (Pa s) and the strain rate $\dot{\epsilon}$ (s^{-1}).

$$S_d = \sigma_d = \mu \cdot \dot{\epsilon} = \mu \cdot \left(\frac{U}{h_d} \right),$$

where U displacement rate (ms^{-1}) and h_d thickness of ductile/viscous material (m).

For rock salt with an almost Newtonian type viscosity $\mu_n \approx 10^{18} \text{ Pa s}$ (Nalpas and Brun, 1993), $h_d = 100 \text{ m}$ and a displacement rate of $U_n = 3 \times 10^{-11} \text{ ms}^{-1}$ ($= 1 \text{ mma}^{-1}$) applied, one obtains

$$S_d(\text{nature}) = \mu_n \cdot \left(\frac{U_n}{h_d} \right) = 3 \times 10^5 \text{ Pa.}$$

This value is in good agreement with the strength values for rock salt, ranging from 0.1–1 MPa, as reported by Carter and Hansen (1983).

In the experiment, we used silicone putty (“Rhodorsil Gum”, manufactured by Rhone Poulenc, Paris) with a Newtonian viscosity $\mu_m \approx 10^4 \text{ Pa s}$, a constant thickness h_d of 5 mm. Applying displacement rates U_m in the range from 1 to 5 cmh^{-1} ($= 2.8 \times 10^{-6}$ – $1.4 \times 10^{-5} \text{ ms}^{-1}$), we obtain values of viscous strength S_d (model) between 5.6 and 28 Pa.

The brittle–viscous strength ratios for the models therefore range from

$$\left(\frac{S_b}{S_d} \right)_{\text{model}} = 14 - 70,$$

whereas the natural counterpart reveals a strength ratio

$$\left(\frac{S_b}{S_d} \right)_{\text{nature}} = \frac{2.2 \cdot 10^7 \text{ Pa}}{3 \cdot 10^5 \text{ Pa}} = 73.$$

The obtained coupling ratios are graphically represented in strength profiles (Fig. 4). Limiting factors in obtaining more precise strength estimates are the uncertainties on salt rheology and its original thickness during rifting. The estimation of strength ratios is only valid if the salt behaves as a Newtonian solid and under dry conditions (zero pore pressure). Note also that the calculation is made for the first, transtensional stage of the experiments only, i.e., considering tensile strengths.

References

- Allemand, P., Brun, J.-P., 1991. Width of continental rifts and rheological layering of the lithosphere. *Tectonophysics* 188, 63–69.
- Becker, A., 2000. The Jura Mountains—an active foreland fold-and-thrust belt? *Tectonophysics* 321, 381–406.
- Bergerat, F., Chorowicz, J., 1981. Etude des images Landsat de la zone transformante Rhin-Saône (France). *Geologische Rundschau* 70 (1), 354–367.
- Brace, W.F., Kohlstedt, D.L., 1980. Limits on Lithospheric Stress Imposed by Laboratory Experiments. *Journal of Geophysical Research* 85 (B11), 6248–6252.
- Brun, J.P., Gutscher, M.A., Teams, D.-E., 1992. Deep crustal structure of the Rhine Graben from DEKORP-ECORS seismic reflection data: a summary. *Tectonophysics* 208, 139–147.
- Brun, J.P., Nalpas, T., 1996. Graben inversion in nature and experiment. *Tectonics* 15 (2), 677–687.
- Byerlee, J.D., 1978. Friction of Rocks. In: Byerlee, J.D., Wyss, M.(Eds), *Pure and Applied Geophysics. Contribution to Current Research in Geophysics*, pp. 615–626.

- Campy, M., 1984. Signification dynamique et climatique des formations et terrasses fluviatiles dans un environnement de moyenne montagne. *Bulletin de l'Association française pour l'Etude du Quaternaire* 1, 87–92.
- Carter, N., Hansen, F., 1983. Creep of rocksalt. *Tectonophysics* 92, 275–333.
- Chauve, P., Campy, M., Pernin, C., Morre-Biot, N., 1983. Carte Géologique détaillée de la France, feuille Pesmes, XXXIII-23. Service de la Carte Géologique de la France.
- Coromina, G., Fabbri, O., 2004. Late Paleozoic NE-SW ductile-brittle extension in the La Serre horst, eastern France. *C.R. Geoscience* 336, 75–84.
- Debrand-Passard, S., Courbouleix, S. (Eds), 1984. Synthèse Géologique du Sud-Est de la France, Vol.2: Atlas, 126. BRGM, G3 pp.
- Deichmann, N., Ballarin Dolfin, D., Kastrop, U., 2000. Seismizität der Nord- und Zentralschweiz. NAGRA Technischer Bericht, 00-05. NAGRA, Wettingen, 94pp.
- Diebold, P., Naef, H., 1990. Der Nordschweizer Permokarbondrog. *Nagra informiert* 2, 29–36.
- Doehl, F., 1970. Die tertiären und quartären Sedimente des südlichen Rheingrabens. In: Illies, J.H., Mueller, S. (Eds), Graben Problems. Proceedings of an International Rift Symposium held in Karlsruhe October, 10-12, 1968. E. Schweizerbart'sche, Stuttgart, pp. 56–66.
- Dreyfuss, M., Glangeaud, L., 1950. La vallée de Doubs et l'évolution morphotectonique de la région bisontine. *Annales scientifiques de l'Université de Besançon* vol.5, pp. 2.
- Dreyfuss, M., Kuntz, G., 1970. Carte Géologique détaillée de la France, feuille Gy, XXXIII-22. Ministère de l'industrie et de la recherche, Service Géologique National, Paris.
- Dubois, A., Odonne, F., Massonnat, G., Lebourg, T., Fabre, R., 2002. Analogue modelling of fault reactivation: tectonic inversion and oblique remobilisation of grabens. *Journal of Structural Geology* 24, 1741–1752.
- Fabbri, O., Gaviglio, P., Marquer, D., 2001. Paleotectonic and neotectonic analyses in the Rhine-Bresse transfer zone: Insights and perspectives from preliminary studies in the Besançon and Massif de la Serre areas. In: Dèzes, P. (Ed.), 2nd EUCOR-URGENT Workshop, 7th-11th October, 2001, Abstract Volume, Mont Saint-Odile, France, pp. 36.
- Giamboni, M., Ustaszewski, K., Schmid, S.M., Schumacher, M.E., Wetzel, A., 2004. Plio-Pleistocene transpressional reactivation of Paleozoic and Paleogene structures in the Rhine-Bresse transform zone (Northern Switzerland and Eastern France). *Geologische Rundschau*, online first, DOI: 10.1007/s00531-003-0375-2.
- Goguel, J., Dreyfuss, M., 1967. Carte Géologique détaillée de la France, feuille Besançon, XXXIII-23. Service de la Carte Géologique de la France, Paris.
- Gürler, B., Hauber, L., Schwander, M., 1987. Die Geologie der Umgebung von Basel mit Hinweisen über die Nutzungsmöglichkeiten der Erdwärme, Schweizerische Geologische Kommission, Bern.
- Håring, M., 2001. Horizontale Hauptspannung im Grundgebirge. <http://www.geothermal.ch/>.
- Hubbert, M.K., 1937. Theory of scale models as applied to the study of geologic structures. *Bulletin Geological Society of America* 48, 1459–1520.
- Illies, J.H., 1981. Mechanism of Graben formation. *Tectonophysics* 73 (1–3), 249–266.
- Krantz, R., 1991. Measurements of friction coefficients and cohesion for faulting and fault reactivation in laboratory models using sand and sand mixtures. *Tectonophysics* 188, 203–207.
- Lacombe, O., Angelier, J., Byrne, D., Dupin, J., 1993. Eocene-Oligocene tectonics and kinematics of the Rhine-Saone continental transform zone (Eastern France). *Tectonics* 12 (4), 874–888.
- Laubscher, H., 1961. Die Fernschubhypothese der Jurafaltung. *Eclogae Geologicae Helveticae* 54 (1), 222–282.
- Laubscher, H., 1970. Grundsätzliches zur Tektonik des Rheingrabens. In: Illies, J.H. Mueller, S. (Eds.), Graben Problems. Proceedings of an International Rift Symposium held in Karlsruhe 1968, International Upper Mantle Project. E. Schweizerbart'sche, Stuttgart, pp. 79–86.
- Laubscher, H., 1977. Fold development in the Jura. *Tectonophysics* 37, 337–362.
- Laubscher, H., 1986. The eastern Jura: relations between thin-skinned and basement tectonics, local and regional. *Geologische Rundschau* 75 (3), 535–553.
- Laubscher, H., 1987. Die tektonische Entwicklung der Nordschweiz. *Eclogae Geologicae Helveticae* 80, 287–303.
- Laubscher, H., 1992. Jura kinematics and the Molasse Basin. *Eclogae Geologicae Helveticae* 85 (3), 653–675.
- Laubscher, H., 2003. The Miocene Dislocations in the northern foreland of the Alps: oblique subduction and its consequences (Basel area, Switzerland-Germany). *Jahresbericht und Mitteilungen des oberrheinischen geologischen Vereins* 85, 423–439.
- Laubscher, H., Noack, T., 1997. The deep structure of the Basel Jura. In: Pfiffner, O.A., Lehner, P., Heitzmann, P., Mueller, S., Steck, A. (Eds.), Deep structure of the Swiss Alps. Results of NRP 20. Birkhäuser, Basel, pp. 54–58.
- Liniger, H., 1963. Geologische Beobachtungen in der Ajoie (Berner Jura). *Regio Basiliensis* 4, 39–47.
- Mandl, G., 1988. Mechanics of tectonic faulting. Models and Basic Concepts. *Developments in Structural Geology* 1. Elsevier, Amsterdam 407pp.
- Müller, W.H., Blümling, P., Becker, A., Clauss, B., 1987. Die Entkoppelung des tektonischen Spannungsfeldes an der Jura-Überschiebung. *Eclogae Geologicae Helveticae* 80 (2), 473–489.
- Müller, W.H., Naef, H., Graf, H.R. (Eds.), 2002. Geologische Entwicklung der Nordschweiz, Neotektonik und Langzeitszenarien, Zürcher Weinland. NAGRA Technischer Bericht, 99-08. NAGRA, Wettingen, 226pp.
- Nalpas, T., Brun, J.-P., 1993. Salt flow and diapirism related to extension at crustal scale. *Tectonophysics* 228, 349–362.
- Nalpas, T., Le Douaran, S., Brun, J.P., Unternehr, P., Richert, J.P., 1995. Inversion of the Broad Fourteens Basin (offshore Netherlands), a small-scale model investigation. *Sedimentary Geology* 95, 237–250.
- Nivière, B., Winter, T., 2000. Pleistocene northwards fold propagation of the Jura within the southern Upper Rhine Graben: seismotectonic implications. *Global and Planetary Change* 27, 263–288.
- Nüesch, R., 1991. Das mechanische Verhalten von Opalinuston. PhD Thesis, ETH Zürich, Zürich, 244pp.
- Petit, C., Campy, M., Chaline, J., Bonvalot, J., 1996. Major palaeohydrographic changes in Alpine foreland during the Pliocene-Pleistocene. *Boreas* 25, 131–143.
- Philippe, Y., 1995. Rampes Laterales et Zones de Transfert dans les Chaînes Plissées: Géométrie, Conditions de Formation et Pièges structuraux associés. Ph.D. Thesis, Université de Savoie & Institute Français du Pétrole, Paris, 272pp.
- Plenefisch, T., Bonjer, K., 1997. The stress field in the Rhine Graben area inferred from earthquake focal mechanisms and estimation of frictional parameters. *Tectonophysics* 275, 71–97.
- Reinecker, J., Heidbach, O., Mueller, B., 2003. The 2003 release of the World Stress Map (available online at <http://www.world-stress-map.org>).
- Richard, P., Krantz, R., 1991. Experiments on fault reactivation in strike-slip mode. *Tectonophysics* 188, 117–131.
- Schmidt, C., Braun, L., Paltzer, G., Mühlberg, M., Christ, P., Jacob, F., 1924. Bohrungen von Buix bei Pruntrut und Allschwil bei Basel. *Beiträge zur Geologie der Schweiz*. pp. 74.
- Schreurs, G., Colletta, B., 1998. Analogue modelling of faulting in zones of continental transpression and transtension. In: Holdsworth, R.E., Strachan, R.A., Dewey, J.F. (Eds.), *Continental*

- Transpressional and Transtensional Tectonics. Geological Society Special Publication. Geological Society, London, pp. 59-79.
- Schumacher, M.E., 2002. Upper Rhine Graben: role of preexisting structures during rift evolution. *Tectonics* 21 (1), 1006.
- Tschanz, X., Sommaruga, A., 1993. Deformation associated with folding above frontal and oblique ramps around the rhomb shaped Val-de-Ruz basin (Jura Mountains). *Annales Tectonicae* 7 (1), 53–70.
- Ustaszewski, K., Schumacher, M.E., Schmid, S.M., in press. Contemporaneous faulting and extensional flexuring during Palaeogene rifting—a case study from the southern Upper Rhine Graben. *Geologische Rundschau*.
- Wildi, W., 1975. Die Mettaufer Überschiebung im Aargauischen Tafeljura (Nordschweiz). *Eclogae Geologicae Helveticae* 68 (3), 483–489.